




Deregulation of circRNA hsa_circ_0009109 promotes tumor growth and initiates autophagy by sponging miR-544a-3p in gastric cancer

Weiwei Zhang^{1,2,†}, Qian Yang^{3,†}, Dongchen Qian⁴, Keli Zhao⁵, Chenxue Tang¹ and Shaoqing Ju ^{1,*}

¹Department of Laboratory Medicine, Affiliated Hospital of Nantong University, Nantong, Jiangsu, P. R. China

²Research Center of Clinical Medicine, Affiliated Hospital of Nantong University, Nantong, Jiangsu, P. R. China

³Center of Clinical Laboratory, First Affiliated Hospital of Soochow University, Suzhou, Jiangsu, P. R. China

⁴Department of Anesthesia and Surgery, Affiliated Hospital of Nantong University, Nantong, Jiangsu, P. R. China

⁵Key Laboratory of Interdisciplinary Research, Institute of Biophysics, Chinese Academy of Sciences, Beijing, P. R. China

*Corresponding author. Department of Laboratory Medicine, Affiliated Hospital of Nantong University, No. 20, Xisi Road, Nantong, Jiangsu 226001, China. Tel: +86-513-85052335; Fax: +86-513-85052105; Email: jsq814@hotmail.com

[†]These authors contributed equally to this work.

Abstract

Background: Autophagy death of cancer cells is detrimental to apoptosis induced by therapeutic drugs, which promotes tumor progression to a certain extent. Increasing reports have demonstrated the regulatory role of circular RNAs (circRNAs) in autophagy. Here, we aimed to determine the role of hsa_circ_0009109 in autophagy in gastric cancer (GC).

Methods: The effects of hsa_circ_0009109 on autophagy were examined using quantitative real-time polymerase chain reaction (qPCR), transmission electron microscopy, Western blot, and immunofluorescence. The mechanism of hsa_circ_0009109 regulating the miR-544a-3p/bcl-2 axis was analysed using fluorescence in situ hybridization, dual-luciferase reporter, and rescue experiments.

Results: Functional testing indicated that hsa_circ_0009109 was significantly down-expressed in GC tissues and cell lines. A reduction in cytoplasmic-derived hsa_circ_0009109 could promote GC progression by accelerating cell proliferation, enhancing migration and invasion, inhibiting apoptosis, and accelerating the cell cycle progression. Besides, hsa_circ_0009109 was found to exert the effect of an autophagy inhibitor such as 3-Methyladenine (3-MA), which was manifested by the weakening of the immunofluorescence of LC3B and the reduction in autophagy-related proteins after overexpression of hsa_circ_0009109, while increased autophagosomes were observed after interference with hsa_circ_0009109. Subsequently, the crosstalk between hsa_circ_0009109 and miR-544a-3p/bcl-2 was verified using dual-luciferase reporter assay. The autophagy status was altered under the regulation of the hsa_circ_0009109-targeted miR-544a-3p/bcl-2 axis.

Conclusions: The hsa_circ_0009109 mediated a novel autophagy regulatory network through targeting the miR-544a-3p/bcl-2 axis, which may shed new light on the exploration of therapeutic targets for the clinical treatment of GC.

Keywords: hsa_circ_0009109; circRNA; autophagy; miR-544a-3p; gastric cancer

Introduction

Gastric cancer (GC) remains prevalent worldwide. More than 1,089,103 new cases and 768,793 deaths occurred in 2020, ranking GC as the third leading cause of cancer-associated death [1]. The threat of GC is also very serious in China, and most patients with GC are usually diagnosed in the middle or even advanced stage. Delayed diagnosis and poor prognosis contribute to a 5-year survival rate of nearly 30% [2]. Cancer formation is a process of dynamic changes involving multiple molecules. Applying innovative molecular technology to an in-depth study of the potential mechanism involved in GC development and translating it into clinical application is the goal of current cancer research.

The emergence of non-coding RNAs (ncRNAs) has provided a new perspective on the diagnosis and treatment of GC.

Circular RNAs (circRNAs) are a class of specific non-coding RNAs that do not have a 5' end cap and a 3' end poly(A) tail, and they form a ring structure using covalent bonds [3]. Recent research has proved that circRNAs are involved in tumor initiation and evolution, including GC. Lai *et al.* [4] reported that hsa_circ_0047905, hsa_circ_0138960, and hsa_circ_769015 were candidate oncogenes in GC, and inhibition of these circRNAs could exerted an inhibitory effect on cell proliferation and invasion. Besides, circLMO7 was reported to act as a miR-30a-3p sponge that affects the glutamine metabolism through the

Received: 4 June 2023. Revised: 26 November 2023. Accepted: 24 January 2024

© The Author(s) 2024. Published by Oxford University Press and Sixth Affiliated Hospital of Sun Yat-sen University

This is an Open Access article distributed under the terms of the Creative Commons Attribution-NonCommercial License (<https://creativecommons.org/licenses/by-nc/4.0/>), which permits non-commercial re-use, distribution, and reproduction in any medium, provided the original work is properly cited.

For commercial re-use, please contact journals.permissions@oup.com

WNT2/ β -Catenin pathway to promote the proliferation, migration, and invasion of GC cells [5] whereas some circRNAs are known as tumor-suppressors, and the loss or low expression of these circRNAs may lead to tumorigenesis. For example, circPSMC3 served as a novel circulating biomarker in GC and blocked tumor progression by sponging microRNA (miRNA)-296-5p [6]. Notably, differently from non-coding RNAs in the traditional sense, some circRNAs can participate in GC progression by encoding short peptides, which confers new vitality on circRNAs [7, 8].

Autophagy is a degradative pathway mediated by lysosomes. Autophagy has attracted increasing attention from researchers in recent years, not only because autophagy has been found to be involved in numerous human physiological functions, but also because autophagy is an important risk factor in the progression of many cancers [9]. The paradoxical roles of autophagy in the malignant progression of tumors are emerging. On the one hand, autophagy blocks the proliferation of tumor cells, induces the death of pre-cancerous cells, and inhibits the occurrence of cancer; on the other hand, autophagy provides energy for tumor cells, helps them survive in the harsh tumor microenvironment, and protects them against apoptosis [10–12]. Altered status of circRNA-regulated autophagy may be responsible for some malignant phenotypes of tumors. Lu et al. [13] reported that increasing circCSPP1 catalysed by heterogeneous nuclear ribonucleoprotein L could induce cellular autophagy through the circCSPP1-miR-520h-EGR1 axis, causing the progression of prostate tumor. Besides, circHIPK3 was found to modulate autophagy via miR124-3p-STAT3-PRKAA signaling in STK11-mutant lung cancer, and a high expression ratio between circHIPK3 and linHIPK3 represented a low autophagic flow [14]. However, the specific regulatory network of circRNAs involved in GC progression by autophagy still needs to be revealed. Induction or inhibition of autophagy may play an important role in cancer therapy. We tried to explore more about the mechanism of circRNAs involved in GC progression by autophagy.

DDB1 and CUL4 associated factor 6 (DCAF6, also named NRIP), as a transcriptional cofactor, can enhance the transcriptional activity mediated by nuclear receptors, including the androgen receptor [15]. By searching the circBank database, we found that DCAF6 could form 36 circRNAs of different lengths with normal cleavage. Among them, hsa_circ_0007277 and hsa_circ_0000154 were reported to be downregulated in GC tissues (GEO accession: GSE78092) [16]. We aim to study the circRNA formed by the alternative splicing of DCAF6, called hsa_circ_0009109, ascertain its biological role in GC, and reveal its molecular mechanism involved in GC progression by regulating autophagy. It provides a molecular target for the regulation of autophagy involved in the treatment of GC.

Materials and methods

Sample collection

A total of 80 pairs of GC tissues and their corresponding 5- to 7-cm adjacent non-cancerous tissues were included in this study. Gastric mucosal glands of non-cancerous tissue were evenly distributed. In contrast to GC tissues, the cells had regular morphology, maintained polarity, and the nuclei were located in the basal layer. All patients were surgically treated and pathologically diagnosed with GC at the Affiliated Hospital of Nantong University between December 2016 and November 2022. The patients had not received any radiation therapy or chemotherapy before the hospital operation. Those patients with a previous tumor history

were excluded. The study was approved by the ethics committee of the local hospital (ethical review report number: 2018-L055) and informed consent was obtained from all patients with GC included.

Cell culture and authentication

Human GC cell lines (BGC-823, SGC-7901, AGS, HGC-27, and MKN-45) were cultured in RPMI-1640 medium (Corning; Corning, NY, USA) supplemented with 10% fetal bovine serum (FBS; Gibco; Grand Island, NY, USA). The human normal gastric epithelium cell line GES-1 was cultured in DMEM medium (Corning) containing 10% FBS. All cells were purchased from the Cell Bank of the Chinese Academy of Sciences (Shanghai, China) in March 2022 and were verified using short tandem repeat analysis. The last test was in February 2023.

RNA extraction and qPCR assay

Total RNA from GC cell and tissue samples was extracted by using TRIzol reagent (Invitrogen; Carlsbad, NM, USA). Then the RNA was reverse-transcribed into complementary DNA (cDNA) using a RevertAid RT Reverse Transcription Kit (Thermo Fisher Scientific; Waltham, MA, USA). Quantitative real-time polymerase chain reaction (qPCR) assay was conducted on a LightCycler® 480 real-time PCR system (Roche; Heidelberg, Baden-Württemberg, Germany) in a total volume of 20 μ L. The levels of expression of circRNA and miRNA were normalized to 18S rRNA and U6 snRNA, respectively. The primer sequence of hsa_circ_0009109 was designed by Geneseeed Corporation (Guangzhou, Guangdong, China) and the Bulge-loop™ miRNA Primer of mi544a-3p was designed by RiboBio (Guangzhou, Guangdong, China).

Plasmid construction and transfection

A 279-bp fragment of hsa_circ_0009109 was cloned into the pLCDH-ciR vector to construct the overexpression plasmid by Geneseeed Corporation. Two individual siRNAs of hsa_circ_0009109 (siRNA1 and siRNA2) and corresponding negative control (siNC) were synthesized by GenePharma Corporation (Suzhou, Jiangsu, China). For cell transfection, cells in log phase could be evenly seeded in six-well plates and transfected when the density was 60%–70% without contamination. The Lipofectamine 3000 (Thermo Fisher Scientific) was used according to the manufacturer's protocol.

CCK-8 and colony formation assays

The transfected cells were seeded into 96-well plates at a density of 4×10^3 cells per well. At Days 1, 2, 3, 4, and 5 after seeding, cell proliferation was measured by adding 10 μ L to the CCK-8 kit (DOJINDO; Kumamoto city, Kumamoto Prefecture, Japan). Then the absorbance value was measured at 450 nm after 2 h of incubation by using a microplate reader. For colony formation assays, 400 cells were seeded per well in a six-well plate and cultured routinely. When the cell colony was visible to the naked eye (in \sim 14 days), the culture was terminated. The colonies were then fixed using 4% paraformaldehyde and stained with 0.05% crystal violet (Beyotime; Shanghai, China).

Cell apoptosis and cell cycle assay

The cells after 48-h transfection were collected and washed twice using cold phosphate buffered saline (PBS). For cell apoptosis assay, cells were stained using the Annexin V PE/7-AAD Apoptosis Detection Kit (BD Pharmingen; San Diego, CA, USA) and incubated in the dark at room temperature for 15 min. For cell cycle assay, cells were fixed using 70% alcohol overnight at 4°C and

then treated using Ribonuclease A (RNase A; Solarbio; Beijing, China) for 30 min. Cells were first stained with propidium iodide for 15 min before detection using flow cytometry.

Transwell assay

For migration assay, the transfected cells (5×10^4 cells) were resuspended using 100 μ L of RPMI-1640 medium and then seeded in the upper chamber (8- μ m pore size; Corning). For invasion assay, the transwell chamber was pre-coated using diluted Matrigel (BD Biosciences; San Jose, CA, USA). The lower chambers were filled with RPMI-1640 medium containing 20% FBS. After 24-h migration and 48-h invasion, the cells on the outer surface of the chamber were fixed and stained with 0.05% crystal violet.

FISH and RNA nucleoplasm separation

Fluorescence *in situ* hybridization (FISH) probes for the hsa_circ_0009109, U6 snoRNA, and 18S rRNA were designed and synthesized by RiboBio. As for the RNA nucleoplasm separation assay, the nuclear and cytoplasmic fraction of SGC-7901 and MKN-45 cells was isolated by using the PARIS™ kit (Ambion; Austin, TX, USA).

Western blot analysis

Total cell protein was lysed in radio immunoprecipitation assay (RIPA) buffer containing protease and phosphatase inhibitor. The protein was then mixed with the loading buffer, separated using sodium dodecyl sulfate–polyacrylamide gel electrophoresis (SDS–PAGE; New Cell & Molecular Biotech; Suzhou, Jiangsu, China), and then transferred onto polyvinylidene fluoride membranes. An enhanced NcmECL Ultra (New Cell & Molecular Biotech) was adopted to visualize the protein bands after incubation with specific antibodies. The antibodies against CYCLIN D1, P27, BCL-2, BAX, BECLIN-1, LC-3, and P62 were purchased from Abcam (Cambridge, MA, USA), and the antibodies against CLEAVED CASPASE 3 and CLEAVED CASPASE 8 were from Cell Signaling Technology (Danvers, MA, USA).

Dual-luciferase reporter assay

Both the full-length and mutant sequences of hsa_circ_0009109 or 3'-UTR of bcl-2 were packed into the psiCHECK™-2 Vector (Promega; Madison, WI, USA) by Genesee Corporation. The constructed luciferase vectors and miR-544a-3p mimics were then co-transfected into GC cells. After 48-h transfection, cells were lysed in passive lysis buffer (Promega) and the luciferase activity was measured using a Thermo Scientific™ Varioskan™ LUX microplate reader (Thermo Fisher Scientific).

Xenograft model in nude mice

Nude mice (BALB/c Nude, 4 weeks old) were purchased from the Laboratory Animal Centre of Nantong University (Nantong, Jiangsu, China). To obtain stable GC cells overexpressing hsa_circ_0009109, the pLCDH-ciR plasmid and two auxiliary plasmids (Pxpax2 and PMD2.G) were used to construct lentivirus overexpression vector (hereinafter represented by LV-pLCDH-ciR). Approximately 5×10^6 BGC-823 cells infected with the empty vector or LV-pLCDH-ciR were suspended in 100 μ L of serum-free RPMI 1640 medium, and subcutaneously inoculated into the flanks of each mouse. Tumor growth was recorded weekly and calculated according to the equation: $0.5 \times \text{length} \times (\text{width})^2$. A month later, the mice were euthanized and the resected tumors were harvested for qPCR and immunohistochemical analysis.

Immunohistochemistry

Formalin-fixed paraffin-embedded tissues were cut into 4- μ m-thick slides. Citrate buffer (0.01 M, pH 6.0) was used for antigen retrieval and 3% H₂O₂ was utilized to block the activity of endogenous peroxidase. Sufficient diluted primary antibody was added and then incubated overnight at 4°C. The slides were washed using PBS, incubated with secondary antibody for 1 h at room temperature, and stained with 3,3'-diaminobenzidine.

Immunocytochemistry

Cells were seeded on glass coverslips and cultured for 24 h. Cells were fixed using 4% paraformaldehyde for 15 min. After immersing the slides three times in PBS, they were permeated with 0.5% Triton X-100 for 20 min at room temperature. Cells were blocked with 5% bovine serum albumin for 30 min and incubated with primary antibodies (anti-LC3B and anti-LAMP1; Cell Signaling Technology) at 4°C overnight. The fluorophore-labeled secondary antibody solution (Invitrogen) was placed on the glass coverslips and incubated for 1 h. For nuclear staining, 4',6-diamidino-2-phenylindole (DAPI) staining solution was added to the slides and specimens incubated for 5 min in the dark.

Statistical analysis

The SPSS v23.0 (IBM; Armonk, NY, USA) and GraphPad Prism v7 (GraphPad Inc.; La Jolla, CA, USA) software were used in this study. All data were analysed on the basis of three biological replicates and were presented as the mean \pm standard deviation (SD). Student's *t*-test was used to compare the means of two groups. When more than three groups existed, ANOVA was applied. The clinicopathological parameters were analysed using the Mann–Whitney *U* test. Spearman correlation analysis was used to reveal the correlation between hsa_circ_0009109 and miR-544a-3p. A *P*-value of <0.05 was deemed statistically significant.

Results

Methodological verification of hsa_circ_0009109 cyclization structure and RNA stability

The hsa_circ_0009109, also known as hsa_circDCAF6_003, was located at chr1: 167935866–167944253 (strand: +). By searching the UCSC Genome Browser on Human (GRCh37/hg19), we found that hsa_circ_0009109 was a kind of exon-derived circRNA, and its breakpoint was located at the beginning of exon 3 and the end of exon 4 of DCAF6, which formed a mature transcript of 279 bp in length (Figure 1A). A specific divergent primer (also known as back-to-back primer) for the hsa_circ_0009109 was first designed to obtain a 131-bp product. Subsequently, agarose gel electrophoresis proved that the size of the PCR amplification product was consistent with the predicted gene product size (Figure 1B). Sanger sequencing validated the cyclization site of hsa_circ_0009109 (Figure 1C). Knowing that divergent primers can only amplify circRNAs, a pair of convergent primers (also called head-to-head primers) were designed that could simultaneously amplify linear parental genes and circRNAs. Both genomic DNA (gDNA) and cDNA were used as templates. The result implied that the divergent primer specifically amplified hsa_circ_0009109 in cDNA, indicating that hsa_circ_0009109 had a ring structure (Figure 1D). RNase R is a 3'–5' exonuclease that cleaves RNA into dinucleotides and trinucleotides from the 3'–5' direction. RNase R digestion assay showed that hsa_circ_0009109 was more stable and resistant to degradation of RNase R compared with DCAF6 (Figure 1E).

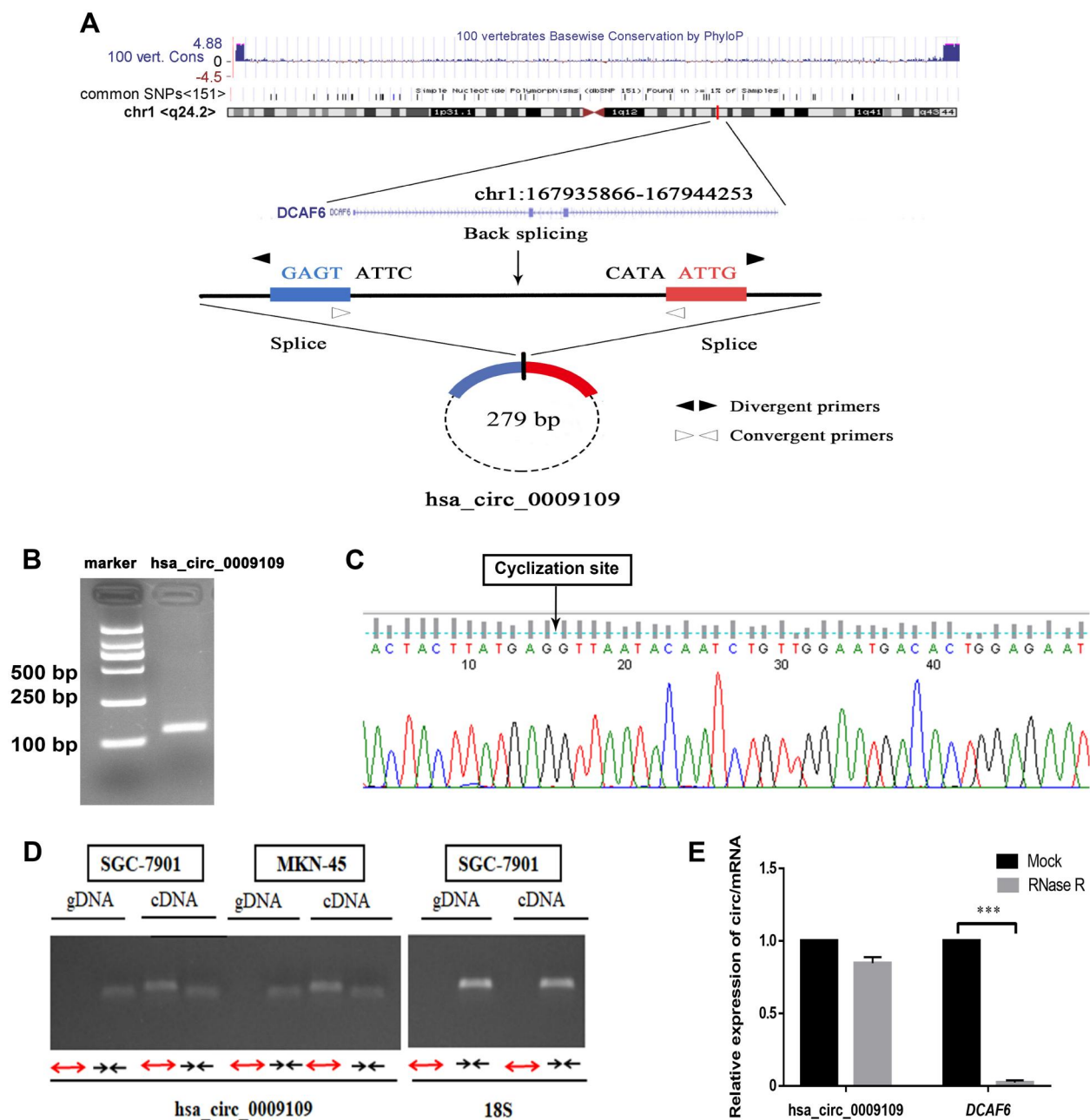


Figure 1. Methodological evaluation of the characteristics of hsa_circ_0009109 in GC. (A) Schematic diagram of hsa_circ_0009109 formation. Arrows represent convergent primers and divergent primers designed for hsa_circ_0009109 amplification. (B) PCR products detected using agarose gel electrophoresis analysis. A single band with the length of 131 bp is shown. (C) Verification of the cyclization site of hsa_circ_0009109 using Sanger sequencing. (D) Verification of the loop structure of hsa_circ_0009109 with convergent primers and divergent primers. (E) RNA exonuclease digestion assay. The data are presented as the mean \pm SD. *** $P < 0.001$. GC = gastric cancer, SD = standard deviation.

Hsa_circ_0009109 suppresses tumor progression in GC

We first performed qPCR in 80 pairs of GC tissue samples and found that the expression of hsa_circ_0009109 was significantly more decreased in cancerous tissues than in the paired non-cancerous tissues (Figure 2A). Next, the downregulation of hsa_circ_0009109 in five GC cells relative to GES-1 cells was confirmed (Figure 2B). The qPCR test showed that the knock-down and overexpression efficiency of hsa_circ_0009109 were in line with expectations in GC cells (Figure 2C). The results of cell proliferation experiments indicated that cell growth of SGC-7901 and MKN-45 was accelerated after silencing hsa_circ_0009109

(Figure 2D and E). Besides, the decrease in hsa_circ_0009109 also facilitated cell migration and invasion (Figure 2F). Flow cytometry and Western blot analysis showed decreased apoptosis and accelerated cell cycle after hsa_circ_0009109 interference, with decreased expression of CLEAVED CASPASE 3, CLEAVED CASPASE 8, BAX, and P27, and increased expression of CYCLIN D1 (Figure 2G–I) whereas hsa_circ_0009109 overexpression inhibited GC progression by slowing down cell proliferation, migration, invasion, and cell cycling via a caspase-dependent apoptotic pathway (Figure 2D–I). In addition, analysis of the clinical pathological parameters revealed a strong association between hsa_circ_0009109 and tumor invasion depth (Table 1). These findings

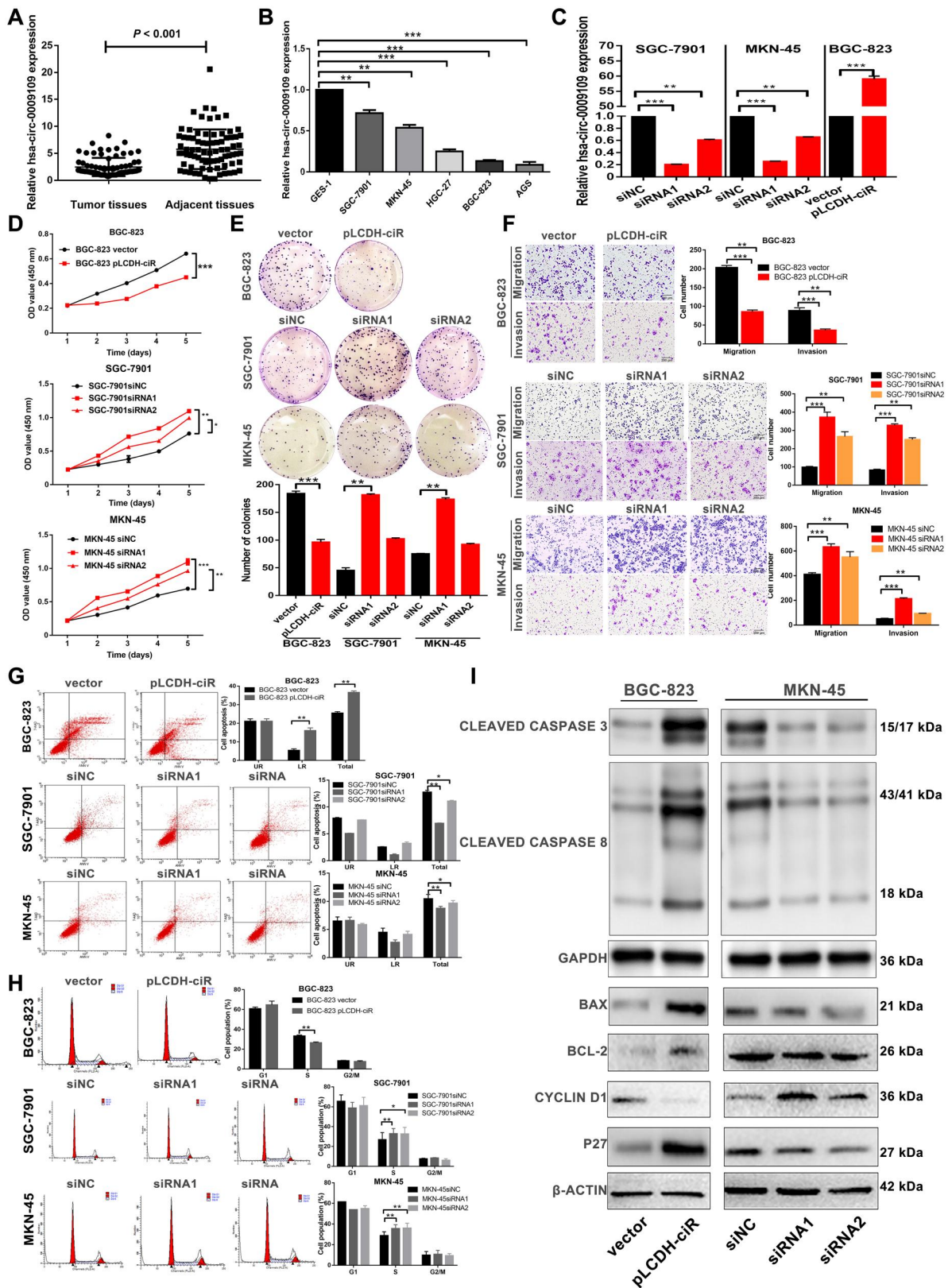


Figure 2. Biological role of hsa_circ_0009109 in GC cells. (A) The expression of hsa_circ_0009109 in 80 pairs of GC tissues and matched non-cancerous tissues. (B) qPCR assay demonstrated downregulation of hsa_circ_0009109 expression in five GC cells relative to GES-1 cells. (C) Verification of transfection efficiency using qPCR. (D) and (E) Detection of the cell proliferation ability by CCK-8 and colony formation assays. (F) Measurement of the cell migration and invasion abilities using the transwell assay. Testing of the cell apoptosis rate (G) and cell cycle progression (H) using flow cytometry. (I) The expression of cell cycle- and apoptosis-associated proteins. GAPDH is used as the internal reference of CLEAVED CASPASE 3 and 8, and β -ACTIN is used for the remaining proteins. The data are presented as the mean \pm SD. * $P < 0.05$; ** $P < 0.01$; *** $P < 0.001$. UR = upper right, LR = lower right, OD = optical density, GC = gastric cancer, SD = standard deviation.

Table 1. Association between hsa_circ_0009109 and clinicopathological characteristics in 80 patients with GC

Characteristic	n	hsa_circ_0009109 expression		P-value
		High (n = 40)	Low (n = 40)	
Sex				
Male	63	32	31	0.785
Female	17	8	9	
Age (years)				
≥60	55	28	27	0.809
<60	25	12	13	
Tumor size (cm)				
≥5	21	7	14	0.075
<5	59	33	26	
Histological differentiation				
Poor	44	20	24	0.369
Moderate	36	20	16	
Lymph node metastasis				
Yes	42	18	24	0.179
No	38	22	16	
Tumor depth				
T3 + T4	55	21	34	0.002**
T1 + T2	25	19	6	

* P < 0.05; ** P < 0.01; *** P < 0.001.

GC = gastric cancer.

suggested that hsa_circ_0009109 played a tumor-suppressive role in GC progression.

Hsa_circ_0009109 overexpression blocks tumor growth in vivo

The biological effect of hsa_circ_0009109 on tumor growth was investigated by establishing a xenograft tumor model in nude mice using lentivirus. Compared with the control group, an increased expression of hsa_circ_0009109 significantly blocked tumor growth (Figure 3A). The qPCR assay showed that the expression of hsa_circ_0009109 was increased significantly in the subcutaneous xenograft of the hsa_circ_0009109-overexpressed group, which further proved that the model that we built was credible (Figure 3B). Besides, the hsa_circ_0009109-overexpressed group showed lower tumor growth and lighter tumor weight than the control group did (Figure 3C and D). Hematoxylin and eosin (H&E) staining showed that the cell structure of the hsa_circ_0009109-overexpressed group was ambiguous; there was cell necrosis such as cytoplasmic dissolution and nuclear fragmentation (Figure 3E). Immunohistochemistry analysis of Ki67 indicated that tumor growth was blocked upon hsa_circ_0009109 overexpression (Figure 3F). In addition, overexpression of hsa_circ_0009109 increased both CLEAVED CASPASE 3 and CLEAVED CASPASE 8, indicating that cell apoptosis was activated (Figure 3G and H).

MiR-544a-3p is sponged by hsa_circ_0009109 in GC

Different subcellular localizations determine the different roles of circRNAs in gene regulation. The results of the RNA nucleoplasmic separation test implied that hsa_circ_0009109 was mainly located in cytoplasm (Figure 4A). The FISH assay further confirmed this conclusion, suggesting that hsa_circ_0009109 may be involved in GC progression via post-transcriptional regulation (Figure 4B). The full-length sequence of hsa_circ_0009109

was first blasted in the circBank (<http://www.circbank.cn/>) and miR-544a-3p with a high score was selected according to miRanda (<http://www.microna.org/microna/home.do>) and TargetScan (<http://www.targetscan.org/>) databases. The expression of miR-544a-3p was relatively high in five GC cells compared with that in GES-1 cells (Figure 4C). Besides, the level of expression of miR-544a-3p was decreased in hsa_circ_0009109-overexpressed BGC-823 cells, whereas knock-down of hsa_circ_0009109 induced an increase in miR-544a-3p expression in SGC-7901 cells (Figure 4D). In addition, miR-544a-3p expression was also found to be upregulated in 58 pairs of GC tissues (Figure 4E). Spearman correlation analysis revealed a negative correlation between miR-544a-3p and hsa_circ_0009109 expression (Figure 4F). Knowing that hsa_circ_0009109 has a sequence complementary to the seed region of miR-544a-3p, luciferase plasmid containing the hsa_circ_0009109 sequence and the sequence with mutated binding sites of miR-544a-3p was constructed. Dual-luciferase reporter assay suggested a decreased luciferase activity in the wild-type group compared with the mutant-type group (Figure 4G). These results suggested that hsa_circ_0009109 sponges miR-544a-3p via the complementary seed region.

Hsa_circ_0009109 inhibits the malignant phenotype of GC cells via negative regulation of miR-544a-3p

To evaluate the role of the hsa_circ_0009109/miR-544a-3p axis in GC progression, rescue experiments, including CCK-8, colony formation, and flow cytometry assays, were designed in BGC-823 cells. CCK-8 assay indicated that miR-544a-3p mimics weakened the proliferation inhibition effect caused by overexpression of hsa_circ_0009109 (Figure 5A and B). Furthermore, transfection of miR-544a-3p mimics accelerated cell cycle progression and increased the proportion of cells in the S-phase, while overexpression of hsa_circ_0009109 reversed the effects above (Figure 5C). In addition, hsa_circ_0009109 overexpression attenuated the anti-apoptotic effect induced by miR-544a-3p mimics and increased the overall proportion of cell apoptosis (Figure 5D). These findings indicated that the tumor-suppressive hsa_circ_0009109 to some extent eliminated the oncogenic effect mediated by miR-544a-3p in GC.

Hsa_circ_0009109 suppresses autophagy via miR-544a-3p/bcl-2 axis in GC

Next, two bioinformatics websites (GEO and TargetScan) were used to identify the downstream signal regulated by the hsa_circ_0009109/miR-544a-3p axis, and BCL-2 was then selected. The dual-luciferase reporter assay disclosed the presence of a specific complementary sequence between miR-544a-3p and BCL-2 (Figure 6A). Knowing that BCL-2 could repress the formation of autophagosomes by directly inhibiting the Beclin-1 and downstream LC3-II, we then assessed the exact role of hsa_circ_0009109 in autophagy.

Hsa_circ_0009109 overexpression led to the upregulation of BCL-2 expression and downregulation of autophagy-related genes such as Beclin1, ATG3, ATG5, ATG7, ATG10, and ATG12, while hsa_circ_0009109 silencing showed the opposite effect (Figure 6B and C). Immunocytochemistry and Western blot analysis revealed that overexpression of hsa_circ_0009109 inhibited the formation of autophagosomes, and the combined treatment with 3-methyladenine (3-MA) enhanced its effect on autophagy (Figure 6D and E). Moreover, more autophagosomes

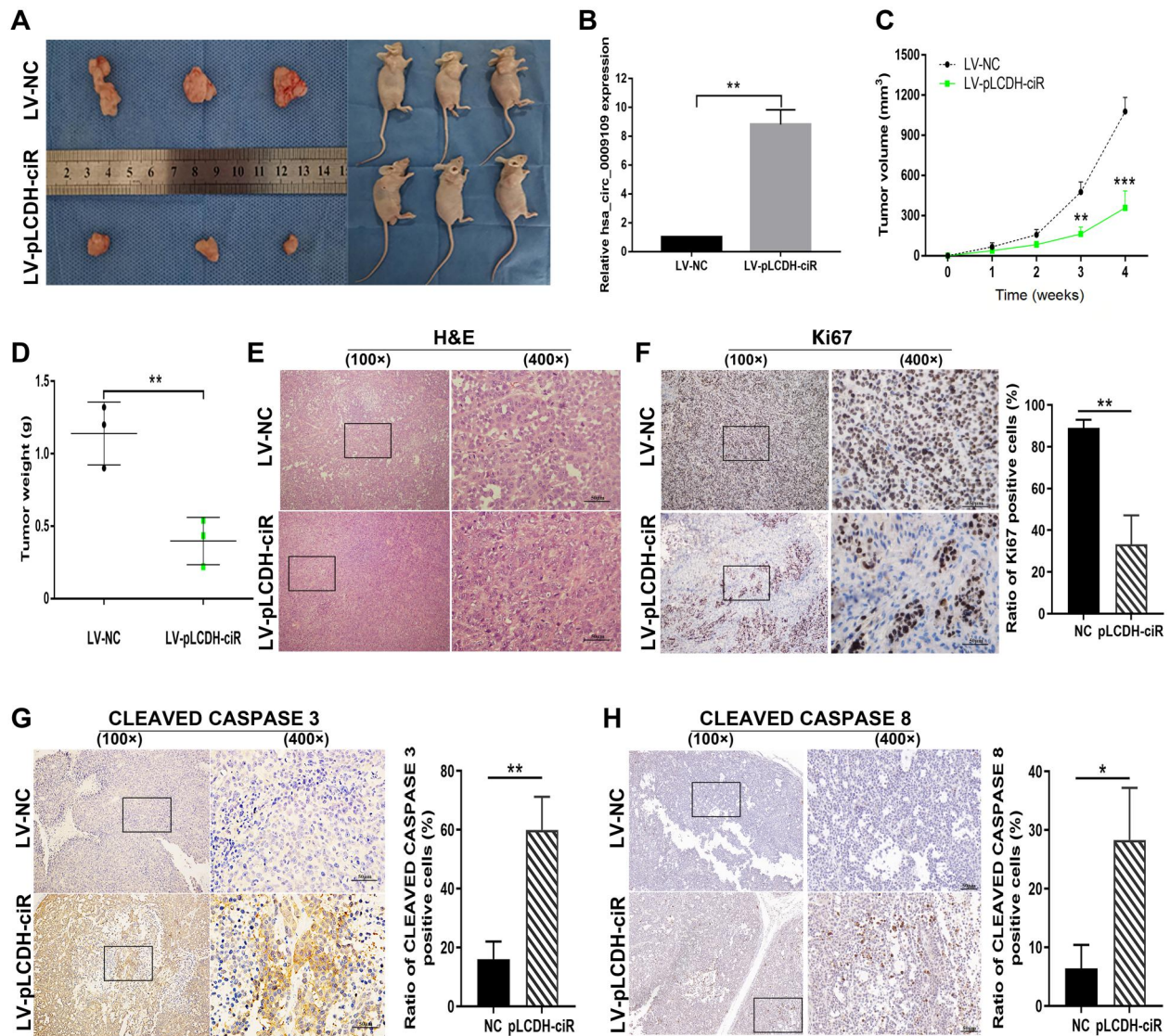


Figure 3. Overexpression of hsa_circ_0009109 blocks tumor growth in the xenograft model. (A) Representative images of subcutaneous xenografts in nude mice in the hsa_circ_0009109 overexpression group (LV-pLCDH-ciR) and empty vector group (LV-NC). (B) The expression of hsa_circ_0009109 in resected tumors of nude mice. (C) A growth curve of the tumor growth in nude mice. The volume of subcutaneous xenografts was recorded every week. (D) The tumor was weighed after subcutaneous xenografts resection. (E) H&E staining of the resected tumors. (F)–(H) Expression levels of Ki67, CLEAVED CASPASE 3, and CLEAVED CASPASE 8 using immunohistochemistry. The data are presented as the mean \pm SD. ** $P < 0.01$, *** $P < 0.001$. H&E = hematoxylin and eosin, SD = standard deviation.

were found in the hsa_circ_0009109 silence group by using transmission electron microscopy (Figure 6F). We also noticed that both knock-down and overexpression of hsa_circ_0009109 affected the formation of autophagosomes, indicating its autophagy regulation function (Figure 6G). In addition, overexpression of hsa_circ_0009109 reduced the number of autophagosomes in BGC-823 cells, but it was abrogated by miR-544a-3p mimics; the increased autophagosomes induced by hsa_circ_0009109 knock-down was also restored by the inhibitor of miR-544a-3p (Figure 6H). Further investigation using Western blotting also demonstrated the regulatory mechanism of hsa_circ_0009109 and miR-544a-3p on autophagy (Figure 6I). Overall, these data suggested that hsa_circ_0009109 regulated cell autophagy mainly through the miR-544a-3p/bcl-2 axis.

Discussion

GC is one of the main deadly malignancies worldwide, posing a significant threat to human health and life. Our aim was to investigate the mechanism of hsa_circ_0009109 in the progression of GC. In our study, hsa_circ_0009109, a specific circRNA formed by alternative splicing of DCAF6, was significantly downregulated in GC tissues and cell lines, and its expression correlated with tumor invasion depth. Functional tests showed that hsa_circ_0009109 silencing promoted cell growth, migration, invasion, and cell cycle in vitro, and overexpressed hsa_circ_0009109 acted as a tumor suppressor in GC cells. Besides, the nude mice model further proved the above findings in vivo. Different subcellular locations of circRNAs determine their various abilities in gene regulation. In our study, the presence of a large proportion of hsa_circ_0009109 in the cytoplasm was observed, implying that hsa_circ_0009109

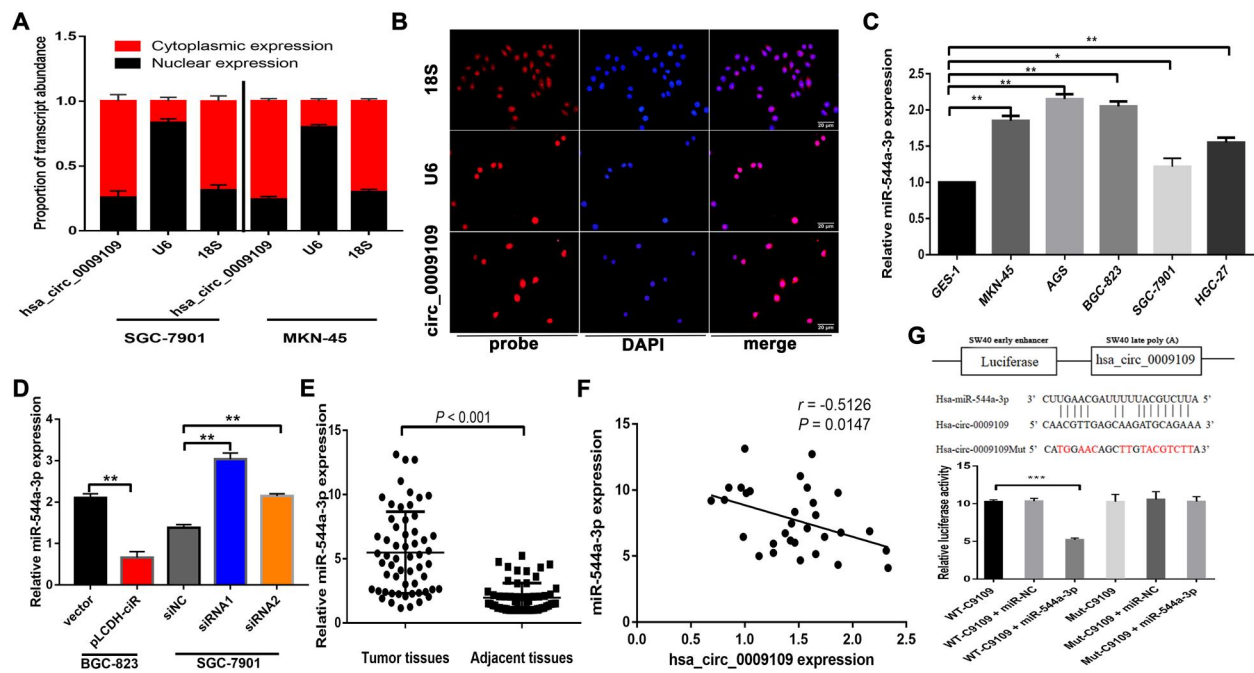


Figure 4. miR-544a-3p is sponged by hsa_circ_0009109 in GC. (A) Detection of hsa_circ_0009109 location in SGC-7901 and MKN-45 cells using nucleoplasm separation assay. (B) Localization of hsa_circ_0009109 using FISH in SGC-7901 cells. (C) The expression of miR-544a-3p in five GC cells. (D) Expression of miR-544a-3p in hsa_circ_0009109-overexpressed BGC-823 cells and hsa_circ_0009109-silenced SGC-7901 cells. (E) The expression of miR-544a-3p in 58 pairs of GC tissues. (F) A negative correlation between hsa_circ_0009109 and miR-544a-3p was observed by using Spearman correlation analysis. (G) Putative binding sites of miR-544a-3p to hsa_circ_0009109. The luciferase assay was adopted to verify the bind sites between hsa_circ_0009109 and miR-544a-3 in HEK-293T cells. The data are presented as the mean \pm SD. * $P < 0.05$; ** $P < 0.01$; *** $P < 0.001$. WT = wild-type, MUT = mutant, FISH = fluorescence in situ hybridization, GC = gastric cancer, SD = standard deviation.

may participate in GC progression by acting as a molecular sponge via a post-transcriptional mechanism. Based on this theory, miR-544a-3p was found to have a complementary binding site to hsa_circ_0009109, which was further confirmed using the dual-luciferase reporter assay.

Previous studies have shown that the biological role of miR-544 in cancer is diverse: Sun et al. [17] reported that miR-544 was frequently downregulated in esophageal squamous cell carcinoma, and overexpression of miR-544 increased the sensitivity of tumor cells to cisplatin. The similar tumor-suppressive role of miR-544 was also reported in cervical cancer [18], triple negative breast cancer [19], and anaplastic thyroid cancer [20]; however, miR-544 may also play an oncogenic role, which should not be ignored. For example, miR-544 was reported to promote tumor progression in colorectal cancer by targeting fork-head box O1 [21]. Additionally, increased expression of miR-544 was confirmed in GC tissues and peritoneal metastasis-derived extracellular vesicles, and its transfer from extracellular vesicles to peritoneal cells increased peritoneal metastasis in GC [22]. The diverse function of miR-544 in cancers may be attributed to tumor specificity and different target genes. In our present study, miR-544a-3p played an oncogenic role in GC cells, which is in agreement with the finding of Zhi et al. [23], but the difference is that we confirmed that BCL-2 was a potential target of miR-544a-3p using dual-luciferase reporter assay, and hsa_circ_0009109 could partially attenuate the tumor-promoting effect of miR-544a-3p.

In this study, overexpression of hsa_circ_009109 or silencing of hsa_circ_009109 in GC cell lines had a greater effect on colony formation in GC cell lines than manipulation of miR-544a-3p.

This indicates that hsa_circ-009109 may affect another miRNA. In our previous review [24], there was a summary of the multiple functions of circRNAs, including binding to multiple miRNAs and RNA-binding proteins, and that one circRNA can regulate multiple miRNAs, and similarly, one miRNA can be regulated by multiple circRNAs. Yu et al. [25] found that circRNA cSMARCA5 inhibits HCC growth and metastasis by miR-17-3p and miR-181b-5p promoting TIMP3 expression. Chen et al. [26] found that circERBIN promotes the proliferation, invasion, angiogenesis, and metastasis of colorectal cancer by targeting miR-125a-5p and miR-138-5p. These reported circRNA-associated multiple biological pathways also suggest to us that follow-up experiments on the interaction of hsa_circ-009109 with other miRNAs could be performed. Although hsa_circ_0009109 may regulate other miRNAs, miR-544a-3p was verified to play a major role in the function of hsa_circ_009109 by CCK-8, flow cytometry, immunofluorescence, and Western blot.

Bcl-2 is known to be a pro-oncogene and a molecular switch that regulates the initiation of autophagy. However, in some cases, bcl-2 has been shown to play a paradoxical inhibitory role in the cancer process [27, 28]. In general, bcl-2 overexpression blocks the formation of the autophagy-promoting Beclin1-Vps34 complex, thereby inhibiting autophagy [29]. Here, bcl-2 may be the downstream signal of the hsa_circ_0009109/miR-544a-3p axis. The regulatory effect of hsa_circ_0009109 on autophagy was also demonstrated, i.e. overexpression of hsa_circ_0009109 reduced the number of autophagosomes, inhibited the formation of autophagosomes, and downregulated the autophagy-promoting marker protein, while knock-down of hsa_circ_0009109 showed the opposite effect. Further studies

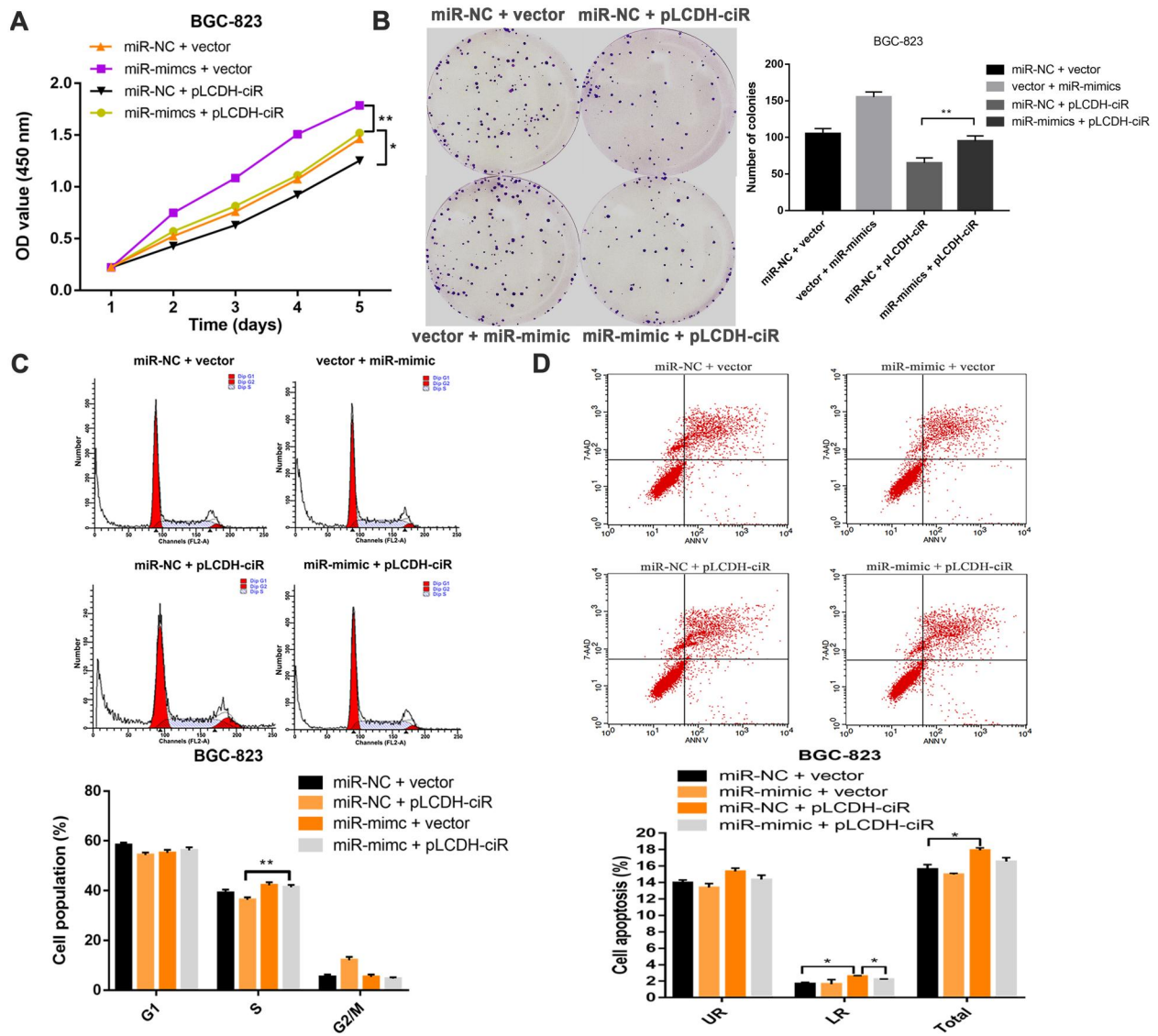


Figure 5. Hsa_circ_0009109 suppresses the malignant phenotype of GC cells via sponging miR-544a-3p. (A) and (B) CCK-8 and colony formation assays were used to evaluate the proliferation ability of BGC-823 cells co-treated with miR-544a-3p mimic (miR-mimic) and overexpression vector (pLCDH-ciR) of hsa_circ_0009109. (C) and (D) Flow cytometry analysis was performed to detect the ratio of cell apoptosis and proportion of cells in the S-phase in dual-transfected BGC-823 cells. All data are presented as the mean \pm SD, * $P < 0.05$; ** $P < 0.01$. UR = upper right, LR = lower right, GC = gastric cancer, SD = standard deviation.

revealed that the miR-544a-3p/bcl-2 axis was involved in the process of hsa_circ_0009109 regulation of autophagy signaling. BCL-2 proteins have anti-apoptotic effects, which may explain the lack of the expected trend in apoptosis experiments by the inverse effect of BCL-2 proteins. In addition, antagonistic effects on BCL-2 protein may also be exerted by other miRNAs regulated by hsa_circ_0009109 in the GC process.

Based on the experimental results, it was hypothesized that the downregulation of hsa_circ_0009109 initiated autophagy and promoted the GC process. Autophagy is an intracellular degradation process in which the autophagic machinery initiates the formation of autophagosomes. Regulation of autophagy plays a dual role in tumor suppression and promotion in many cancers. In cancer cells, autophagy suppresses tumorigenesis by inhibiting cancer cell survival and inducing cell death, but it also promotes tumorigenesis by promoting cancer cell proliferation and

tumor growth [9]. Apoptosis, or programmed cell death, is the natural method of removing senescent cells from the body. Despite a few studies to the contrary [30, 31], it is generally accepted that dysregulation of apoptotic signaling, particularly activation of the anti-apoptotic system, can lead to uncontrolled proliferation of cancer cells, resulting in tumor survival, drug resistance, and cancer recurrence [32]. In the present study, the effect on apoptosis after manipulation of hsa_circ_0009109 was not particularly pronounced; the caspase pathway of apoptosis was mainly mediated by the hsa_circ_0009109/miR-544a-3p axis. Autophagy-related experiments verified that downregulation of hsa_circ_0009109 induced autophagy. Meanwhile, we speculated that the proliferation and tumor growth of GC cells were mainly affected by the enhancement of autophagy, which was consistent with the results of CCK-8, colony formation, and other experiments.

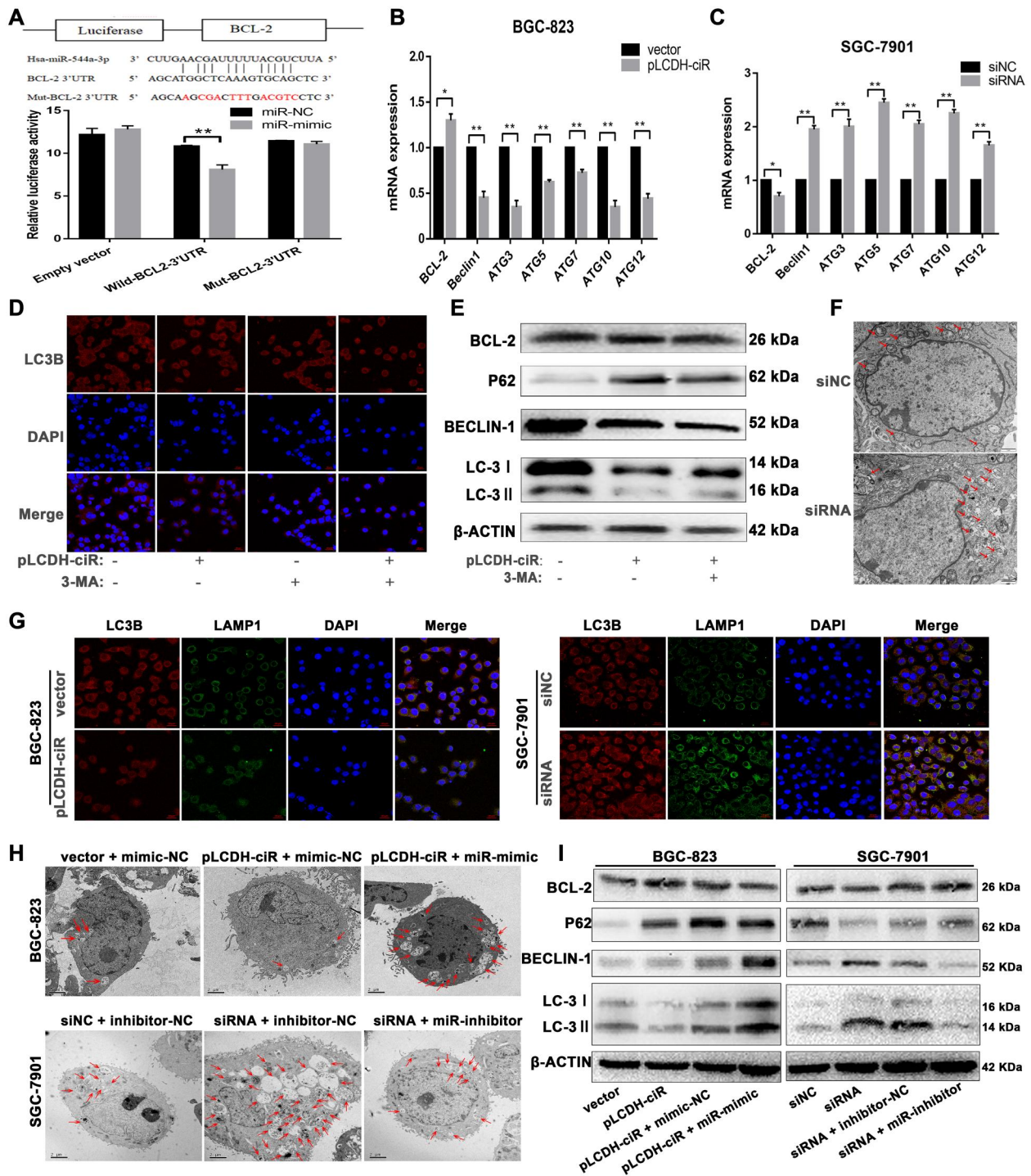


Figure 6. Hsa_circ_0009109 regulates tumor progression through inhibiting autophagy via the miR-544a-3p/bcl-2 axis. (A) Putative binding sites of miR-544a-3p to BCL-2 using TargetScan. The luciferase assay was performed to verify the bind sites between miR-544a-3 and 3'-UTR of BCL-2 in HEK-293 T cells. (B) and (C) The levels of expression of BCL-2, Beclin1, ATG3, ATG5, ATG7, ATG10, and ATG12 were detected using qRT-PCR in hsa_circ_0009109-overexpressed BGC-823 cells and hsa_circ_0009109-silenced SGC-7901 cells. (D) Immunocytochemical analysis of autophagosomes in BGC-823 cells transfected with overexpression vector of hsa_circ_0009109 (pLCDH-ciR) or treated with 3-MA (2 mM). (E) Expression of autophagy-associated proteins in BGC-823 cells co-treated with pLCDH-ciR and 3-MA (2 mM). (F) Autophagosomes viewed using electron microscopy in hsa_circ_0009109-silenced SGC-7901 cells. The arrows point to the typical autophagosomes. (G) Immunocytochemical analysis of autophagosomes and lysosomes. Anti-LC3 and anti-LAMP1 antibodies were used to mark autophagosomes (LC3B, red fluorescent labeling) and lysosomes (LAMP1, green fluorescent labeling), respectively. (H) Autophagosomes in BGC-823 cells and SGC-7901 cells were observed using an electron microscope. (I) Autophagy-related proteins detected using Western blotting. All data are presented as the mean \pm SD. * $P < 0.05$; ** $P < 0.01$. WT = wild-type, MUT = mutant, SD = standard deviation.

Conclusion

In summary, hsa_circ_0009109 was downregulated in GC and negatively associated with tumor depth in patients with GC. Functional tests demonstrated its role as a tumor suppressor, namely inhibition of autophagy through the miR-544a-3p/bcl-2 signaling axis. Thus, hsa_circ_0009109 may prove to be a potential therapeutic target for GC treatment.

Authors' Contributions

W.Z. drafted and revised the paper. Q.Y. and C.T. designed and operated the experiments. D.Q. was responsible for data acquisition and visualization. K.Z. acquired and managed patients. C.T. and S.J. selected the topic and reviewed this paper. All authors read and approved the final manuscript.

Funding

This work was supported by the National Natural Science Foundation of China [nos 82272411, 82072363], Jiangsu Innovative and Entrepreneurial Talent Programme [JSSCBS20211602], PhD Research Startup Foundation of Affiliated Hospital of Nantong University [Tdb2011], Postdoctoral Research Foundation of Affiliated Hospital of Nantong University [BSH202110], Scientific Research Project of Nantong Municipal Health Commission [QN2022015], Nantong Basic Research Program [JC12022007], and Grants from Jiangsu Provincial Research Hospital [YJXY202204-YSC28].

Acknowledgements

We thank Yan Li's group at the Institute of Biophysics, Chinese Academy of Sciences for providing technical guidance.

Conflicts of Interest

The authors declare that there is no conflict of interests in this study.

References

- Sung H, Ferlay J, Siegel RL et al. Global cancer statistics 2020: GLOBOCAN estimates of incidence and mortality worldwide for 36 cancers in 185 countries. *CA Cancer J Clin* 2021;**71**:209–49.
- Chen W, Zheng R, Baade PD et al. Cancer statistics in China, 2015. *CA Cancer J Clin* 2016;**66**:115–32.
- Beermann J, Piccoli MT, Viereck J et al. Non-coding RNAs in development and disease: background, mechanisms, and therapeutic approaches. *Physiol Rev* 2016;**96**:1297–325.
- Lai Z, Yang Y, Yan Y et al. Analysis of co-expression networks for circular RNAs and mRNAs reveals that circular RNAs hsa_circ_0047905, hsa_circ_0138960 and has-circRNA7690-15 are candidate oncogenes in gastric cancer. *Cell Cycle* 2017;**16**:2301–11.
- Cao J, Zhang X, Xu P et al. Circular RNA circLMO7 acts as a microRNA-30a-3p sponge to promote gastric cancer progression via the WNT2/ β -catenin pathway. *J Exp Clin Cancer Res* 2021;**40**:6.
- Rong D, Lu C, Zhang B et al. CircPSMC3 suppresses the proliferation and metastasis of gastric cancer by acting as a competitive endogenous RNA through sponging miR-296-5p. *Mol Cancer* 2019;**18**:25.
- Jiang T, Xia Y, Lv J et al. A novel protein encoded by circMAPK1 inhibits progression of gastric cancer by suppressing activation of MAPK signaling. *Mol Cancer* 2021;**20**:66.
- Zhang Y, Jiang J, Zhang J et al. CircDIDO1 inhibits gastric cancer progression by encoding a novel DIDO1-529aa protein and regulating PRDX2 protein stability. *Mol Cancer* 2021;**20**:101.
- Debnath J, Gammoh N, Ryan KM. Autophagy and autophagy-related pathways in cancer. *Nat Rev Mol Cell Biol* 2023;**24**:560–75.
- He LQ, Lu JH, Yue ZY. Autophagy in ageing and ageing-associated diseases. *Acta Pharmacol Sin* 2013;**34**:605–11.
- Gozuacik D, Kimchi A. Autophagy as a cell death and tumor suppressor mechanism. *Oncogene* 2004;**23**:2891–906.
- Ogier-Denis E, Codogno P. Autophagy: a barrier or an adaptive response to cancer. *Biochim Biophys Acta* 2003;**1603**:113–28.
- Lu J, Zhong C, Luo J et al. HnRNP-L-regulated circCSPP1/miR-520h/EGR1 axis modulates autophagy and promotes progression in prostate cancer. *Mol Ther Nucleic Acids* 2021;**26**:927–44.
- Chen X, Mao R, Su W et al. Circular RNA circHIPK3 modulates autophagy via MIR124-3p-STAT3-PRKAA/AMPK α signaling in STK11 mutant lung cancer. *Autophagy* 2020;**16**:659–71.
- Tsai TC, Lee YL, Hsiao WC et al. NRIP, a novel nuclear receptor interaction protein, enhances the transcriptional activity of nuclear receptors. *J Biol Chem* 2005;**280**:20000–9.
- Shao Y, Li J, Lu R et al. Global circular RNA expression profile of human gastric cancer and its clinical significance. *Cancer Med* 2017;**6**:1173–80.
- Sun F, Zhang C, Ma D et al. MicroRNA-544 inhibits esophageal squamous cell carcinoma cell proliferation and enhances sensitivity to cisplatin by repressing E2F transcription factor 5. *Oncol Lett* 2019;**18**:4203–9.
- Zhu Z, Wang S, Zhu J et al. MicroRNA-544 down-regulates both Bcl6 and Stat3 to inhibit tumor growth of human triple negative breast cancer. *Biol Chem* 2016;**397**:1087–95.
- Wang F, Li Z, Sun B. miR-544 inhibits the migration and invasion of anaplastic thyroid cancer by targeting Yin Yang-1. *Oncol Lett* 2019;**17**:2983–92.
- Yao GD, Zhang YF, Chen P et al. MicroRNA-544 promotes colorectal cancer progression by targeting forkhead box O1. *Oncol Lett* 2018;**15**:991–7.
- Pan C, Xiang L, Pan Z et al. MiR-544 promotes immune escape through downregulation of NCR1/NKp46 via targeting RUNX3 in liver cancer. *Cancer Cell Int* 2018;**18**:52.
- Kong W, Liu X, Yin G et al. Extracellular vesicle derived miR-544 downregulates expression of tumor suppressor promyelocytic leukemia zinc finger resulting in increased peritoneal metastasis in gastric cancer. *Aging (Albany NY)* 2020;**12**:24009–22.
- Zhi Q, Guo X, Guo L et al. Oncogenic miR-544 is an important molecular target in gastric cancer. *Anticancer Agents Med Chem* 2013;**13**:270–5.
- Tao M, Zheng M, Xu Y et al. CircRNAs and their regulatory roles in cancers. *Mol Med* 2021;**27**:94.
- Yu J, Xu QG, Wang ZG et al. Circular RNA cSMARCA5 inhibits growth and metastasis in hepatocellular carcinoma. *J Hepatol* 2018;**68**:1214–27.
- Chen LY, Wang L, Ren YX et al. The circular RNA circ-ERBIN promotes growth and metastasis of colorectal cancer by

- miR-125a-5p and miR-138-5p/4EBP-1 mediated cap-independent HIF-1 α translation. *Mol Cancer* 2020;**19**:164.
27. de La Coste A, Mignon A, Fabre M et al. Paradoxical inhibition of c-myc-induced carcinogenesis by Bcl-2 in transgenic mice. *Cancer Res* 1999;**59**:5017–22.
 28. Murphy KL, Kittrell FS, Gay JP et al. Bcl-2 expression delays mammary tumor development in dimethylbenz(a)anthracene-treated transgenic mice. *Oncogene* 1999;**18**:6597–604.
 29. Pattingre S, Levine B. Bcl-2 inhibition of autophagy: a new route to cancer? *Cancer Res* 2006;**66**:2885–8.
 30. Wang RA, Li QL, Li ZS et al. Apoptosis drives cancer cells proliferate and metastasize. *J Cell Mol Med* 2013;**17**:205–11.
 31. Wang RA, Li ZS, Yan QG et al. Resistance to apoptosis should not be taken as a hallmark of cancer. *Cell Cycle* 2014;**33**:1–50.
 32. Mohammad RM, Muqbil I, Lowe L et al. Broad targeting of resistance to apoptosis in cancer. *Semin Cancer Biol* 2015;**35** Suppl:S78–S103.